COMBUSTOR TURBULENCE

C. John Marek
National Aeronautics and Space Administration
Lewis Research Center
Cleveland, Ohio 44135

The turbulence entering the turbine is produced in the combustor. High turbulence levels from the combustor can alter the location of the transition point on the turbine vane. The dynamics of turbulence and the progress being made in computing the flow are discussed.

The contraction between a combustor (fig. 1) and a turbine inlet can be anywhere from 50 percent on advanced engines to 75 percent (25-percent open area) on older engines. Effective blockages of the combustor are about 75 percent. Combustors operate at reference velocities of 30 m/sec with incoming dilution jet velocities of 120 m/sec.

Only a few measurements have been made of combustor turbulence, and these have usually been at the combustor exit. In 1979 turbulence was measured at the exit of a T-63 combustor (ref. 1) with 75-percent contraction (fig. 2). With combustion and at isothermal conditions, typical turbulence levels were 6 to 10 percent. These data were taken with a laser Doppler velocimetry (LDV) system, and the velocity probability distribution was fitted to a Gaussian (fig. 3). The turbulence intensity is the standard deviation of the sample. At flight idle conditions the turbulence level was 7 percent. The probability distribution tended to be Gaussian over a wide range of velocity. Therefore the probability of an event or of a given velocity being different from the mean could be determined.

Data presented at a recent meeting on hot-section technology (HOST) (fig. 4) show LDV measurements taken at the exit of a combustor in a free jet (fig. 5). Again, the combustor had 75-percent contraction (or 25-percent open area). The nozzle was 50 mm in diameter, and the measurements were taken 60 mm, or 1.2 jet diameters, downstream. In cold flow the turbulence intensity was 8 percent on the centerline and 50 percent at the edge. The higher values show the influence of the mixing wake on turbulence. In hot flow the turbulence intensity was 9 percent in the core region, so it did not increase much with combustion. The exhaust velocity, of course, went from 60 m/sec in cold flow to 220 m/sec with combustion.

For a simple round jet the turbulence intensity was normalized with the centerline velocity, with peak values of 20 percent and dropping off toward the edge (fig. 6(a)). The axial distribution of the maximum turbulence intensity (fig. 6(b)) showed lower values below Z/D = 10, representing the potential core.

The turbulence intensities for a combustor exhaust are about 10 percent for 75-percent contraction. Future engines will probably be designed with close to 50-percent contraction. Turbulence increases with decreasing contraction. For 10-percent turbulence in the exhaust the combustor turbulence would

be 40 percent; so engines with 50-percent contraction would have a turbine inlet turbulence of 20 percent.

A motion picture of the dynamics of combustor turbulence was taken at the University of California, Berkeley. The motion picture (C-315) is available on loan from the NASA Lewis Research Center by sending in the request card at the end of this document. Some still photographs from the motion picture (fig. 7) show large-scale structures. The premixed propane-air flowed at 20 m/sec through a two-dimensional nozzle over a rearward-facing step. The step was 2.5 cm high and 17.8 cm deep. As the fuel-air ratio of the mixture was increased, the flame speed increased. Instability occurred and the flame flashed over the lip. The boundary layer on the nozzle lip went through transition, probably caused by the flow instability arising from the dynamics of the combustion process. The dynamics of the flow is evident in the motion picture. In the next sequence (fig. 7(b)) an additional step was placed in the exhaust to determine the effect of contraction on the turbulence leaving the combustor. The step produced a 50-percent contraction. Amazingly, the turbulence unwound and went straight into the contraction. The size of the turbulence structures was tailored by the duct to the size of the available duct height. Flashback occurred at a different fuel-air ratio than it did without the downstream step. The structure of the flame front and this particular wave were quite different from the flow without the downstream step. The term "wave" is used because of the influence of the downstream step on the flow, which was at the same velocity as in the sequence with the single step. Color schlieren photography at 6000 frames/sec was used, and frame duplication was used to slow down an event. The schlieren system is sensitive to small temperature gradients. In the motion picture the combustion zone is the black region and the regions of unburned gas and the reacted gas underneath the step appear blue.

The final sequences of the motion picture present random vortexes calculated by the method of Chorin. The turbulence is quite dynamic. It is hard to predict the flashback condition. By using the Chorin technique turbulent flow can be computed with and without combustion.

Without combustion large-scale turbulence structures as well as much finer turbulence scales were present (fig. 8). As the Reynolds number increased, the scale of turbulence became finer. Turbulence would be expected to increase with combustion. However, as the temperature rose from 600 to 1600 K the viscosity went up by a factor of 10, so the Reynolds number actually went down. You might then expect that turbulence would decrease.

In a frequency spectrum taken with a high-response pressure transducer just downstream of a typical swirl can combustor, most of the frequencies were below 2000 Hz (fig. 9). Few intense peaks occurred. As the pressure was increased from 700 to 1420 kPa (7 to 14 atm), the Reynolds number and the energy in the higher frequencies increased. In an engine the combustor velocity remains nearly constant and the mass flow increases with pressure. However, with all of the dynamics the turbulence did not change significantly.

The progress being made toward computing turbulence is discussed in detail in references 3 and 4. Reference 3 gives the theoretical background and reference 4 presents the computer program MIMOC used to compute the two-dimensional unsteady flow.

In the MIMOC method two types of finite vortex elements are introduced (fig. 10). A vortex sheet is a line vortex. Sheets are introduced at the wall to satisfy the no-slip boundary condition and to simulate the generation of turbulence at the wall. When a sheet moves out of a boundary layer of thickness δ_s, it becomes a vortex blob and its image. The vortices are moved with a particular variance. The variance of the Gaussian distribution is proportional to the time step and inversely proportional to the Reynolds number. The vortices move a distance ΔZ, which is the sum of the convected distance and the random motion. A reduced-time coordinate system is used. The reduced time τ is the time t multiplied by the inlet channel velocity U_0 and divided by the duct height H. The Reynolds number is also defined in terms of H. The motion of each vortex blob (fig. 11) is computed from the local velocity created by all of the other elements plus the Gaussian random walk.

Comparing the experimental data and the random vortex method shows good agreement for the mean velocities (fig. 12) but poorer agreement for the turbulence intensities normalized by the inlet velocity (fig. 13). Remember that these computations include no turbulence constants but only the turbulence generated by the fundamental equations. Intensity peaks at about 20 to 30 percent in the shear layer for both the nonreacting and reacting flows. The Reynolds number in this comparison is 22 000. For reacting flow the peak in intensity shifted down into the recirculation region and the recirculation region shortened with reaction.

The time history of the calculated velocity at a point in the flow (fig. 14) looks realistic, like the signal from a hot wire. A histogram was made of these points (fig. 15); the distribution looks Gaussian.

When the results were analyzed with a fast Fourier transform (FFT), the frequency spectrum could be plotted (fig. 16). The results are presented in reduced frequency, which is the duct height divided by the inlet velocity. The power is high below 200 Hz, with peaks. Some of the peaks may be caused by the lack of resolution in the calculation. The frequency spectrum rolls off as the experimental data. A power spectral distribution (fig. 17) shows most of the power (75 percent) below a reduced frequency of 1.

The turbulent characteristics of the flow need to be quantified in order to be able to predict transition in turbines. Chorin's method is useful for understanding and predicting vortex flows.

REFERENCES

1. Zimmerman, D.R.: Laser Anemometer Measurements at the Exit of a T63-C20 Combustor. (DDA-RN-79-4, Detroit Diesel Allison; NASA Contract NAS3-21267.) NASA CR-159623, 1979.

2. Seasholtz, Richard G.; Oberle, Lawrence G.; and Weikle, Donald H.: Laser Anemometry for Hot Section Applications. Turbine Engine Hot Section Technology, NASA CP-2289, 1983, pp. 57-67.

3. Ghoniem, A.F.; Chorin, A.J.; and Oppenheim, A.K.: Numerical Modelling of Turbulent Flow in a Combustion Tunnel. Philos. Trans. R. Soc. London, Ser. A, vol. 304, no. 1484, Mar. 9, 1982, pp. 303-325.

4. Ghoniem, Ahmed F.; Marek, Cecil J.; and Oppenheim, Antoni K.: Modeling Interface Motion of Combustion (MIMOC). NASA TP-2132, 1983.

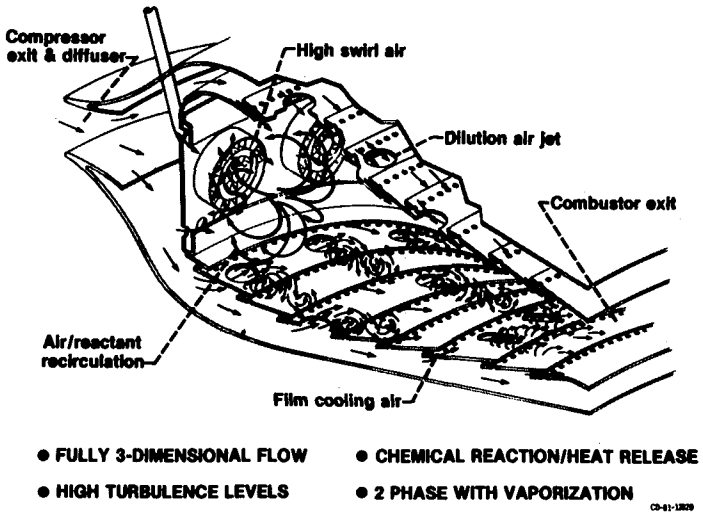

Figure 1. - Combustion flow phenomena.

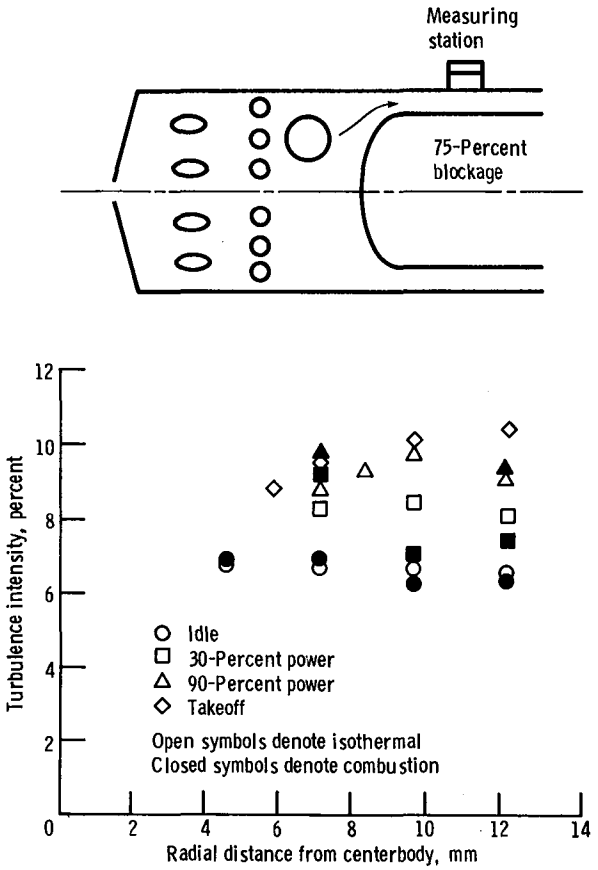

Figure 2. - LDV measurements of turbulence intensity. (From ref. 1.)

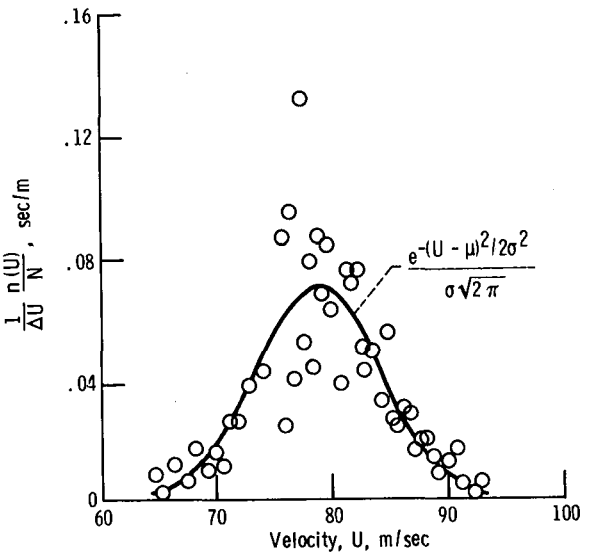

Figure 3. - Determination of turbulence intensity from probability distribution. Flight-idle burning, $r = 7.10$ mm; $\mu = 79.0$ m/s; $\sigma = 5.50$ m/s; $\sigma/\mu = 6.96$ percent; $U_{upper} = 94.0$ m/s; $U_{lower} = 64.0$ m/s; $\langle U \rangle = 79.0$ m/s; $s = 5.61$ m/s; $s/\langle U \rangle = 7.10$ percent; $N = 820$. (From ref. 1.)

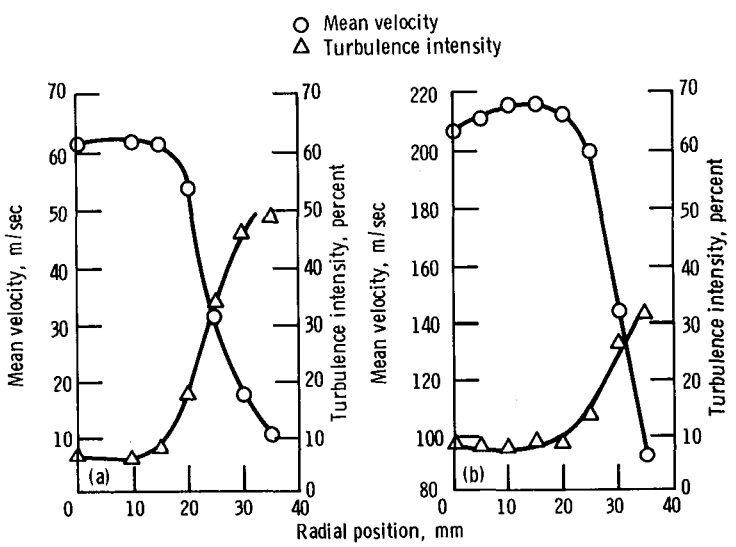

(a) Isothermal. Temperature, 25 °C.
(b) With combustion. Temperature, 780 °C.

Figure 4. - Combustor exhaust measurements. Axial position downstream, 60 mm. (From ref. 2.)

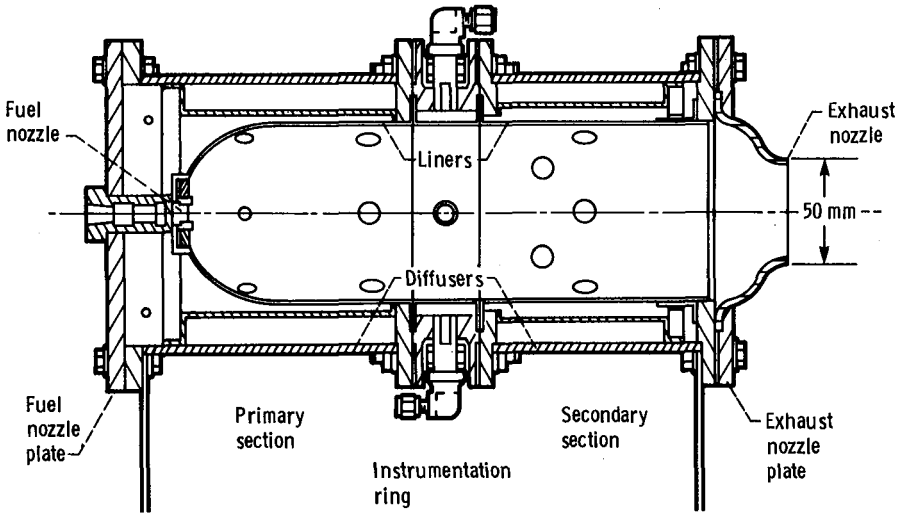

Figure 5. - Laboratory combustor.

CD-85-15972

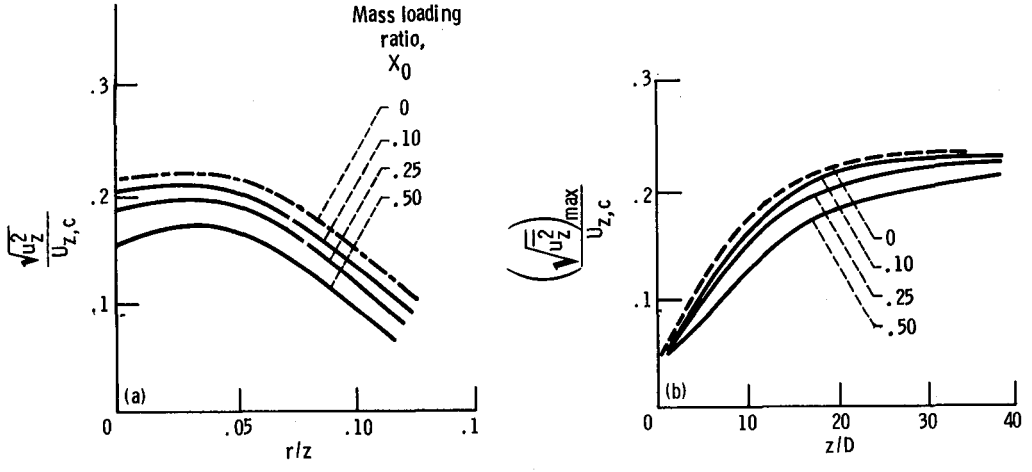

(a) Turbulence intensity distribution at z/D = 20.
(b) Axial distribution of maximum turbulence intensity.

Figure 6. - Turbulence intensity distributions.

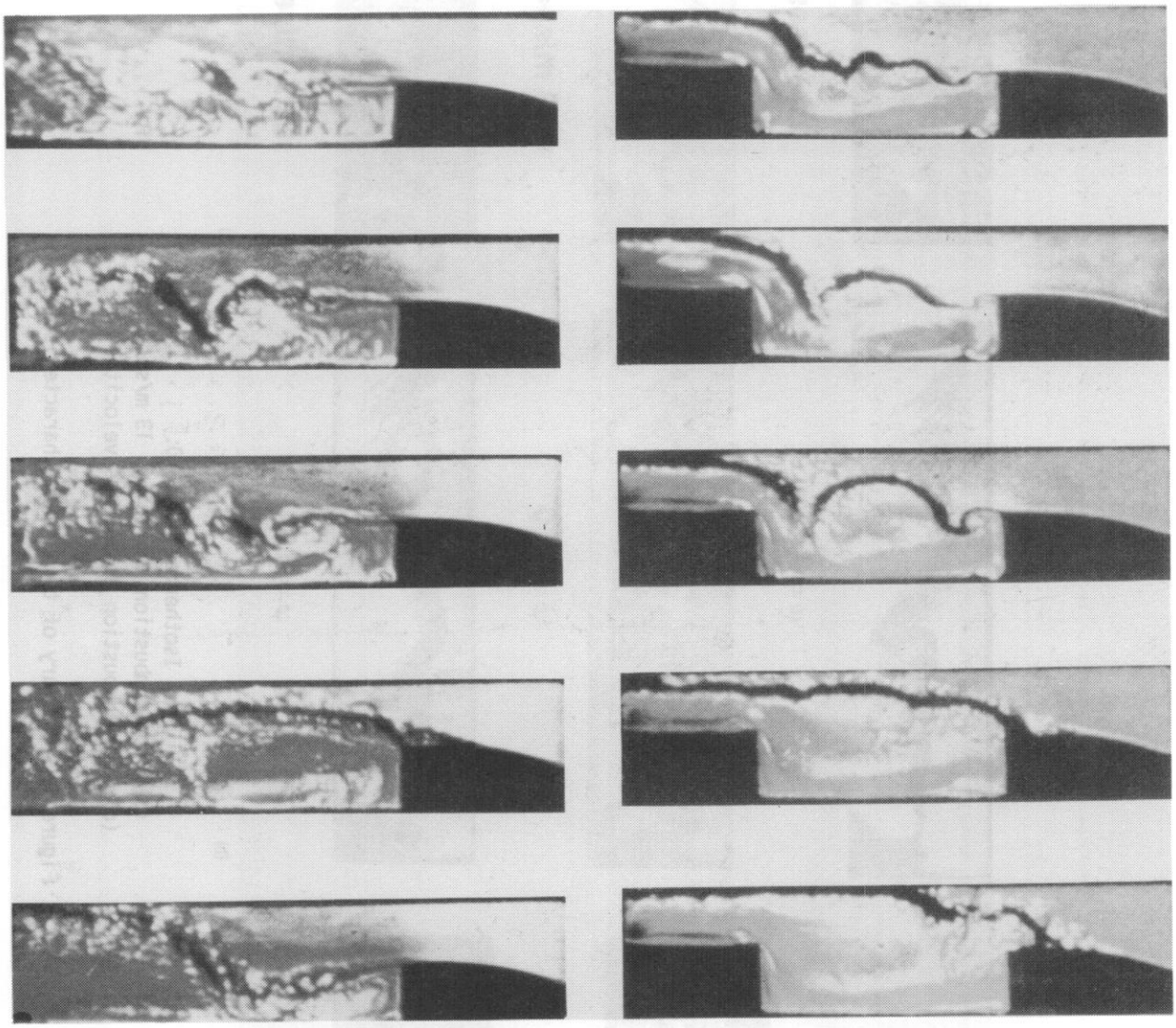

(a) (b)

(a) Sequence 1.
(b) Sequence 2.

Figure 7. - Still photographs of color schlieren motion pictures. (Flow from right to left.)

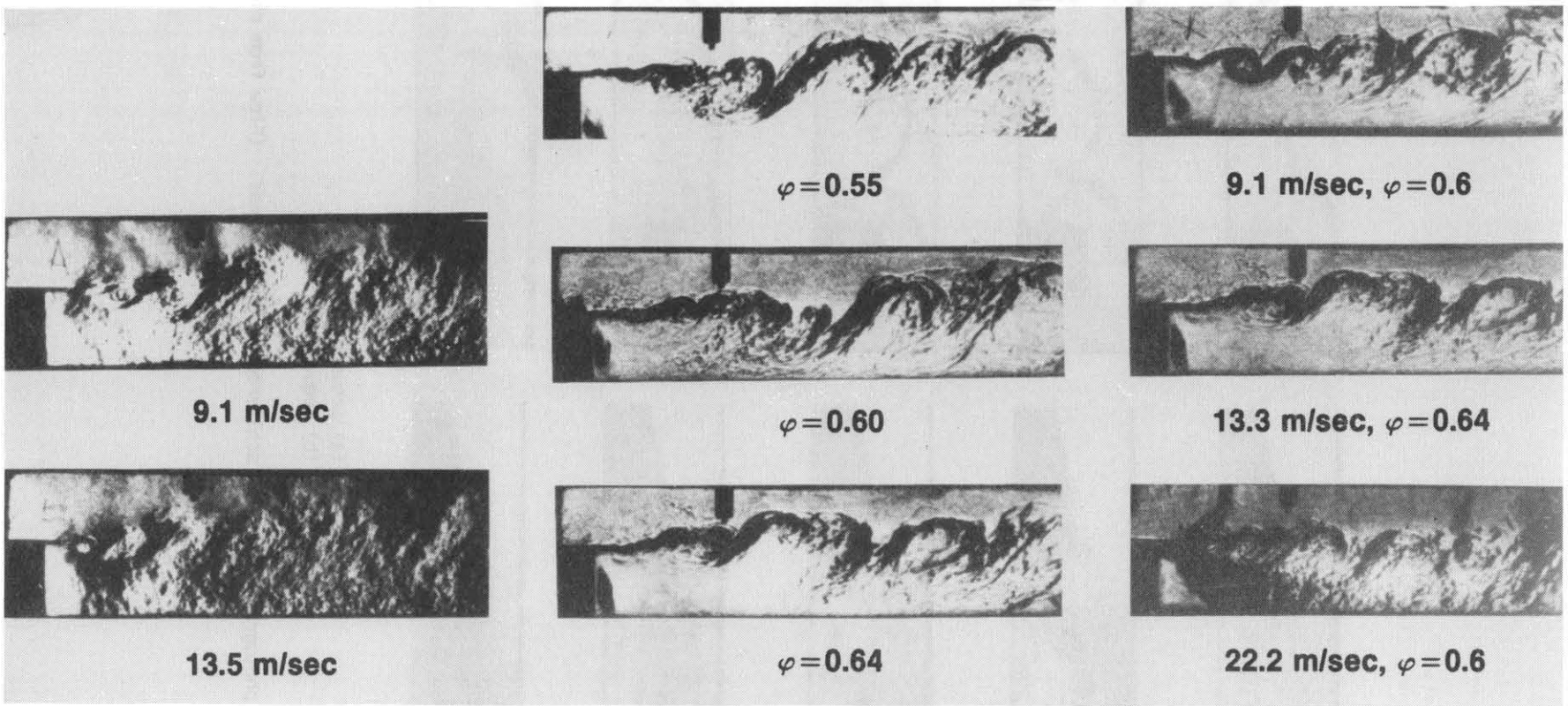

(a) Isothermal; $\varphi = 0$.
(b) With combustion; velocity, 13 m/sec.
(c) With combustion at various velocities.

Figure 8. - Summary of turbulence characteristics.

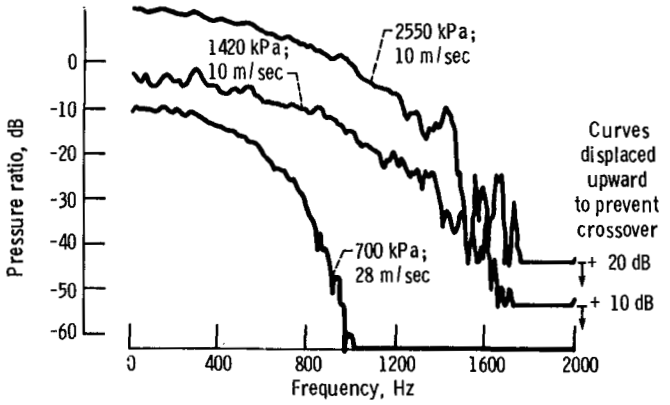

Figure 9. - Frequency spectrum downstream of swirl can combustor. Temperature, 550 K.

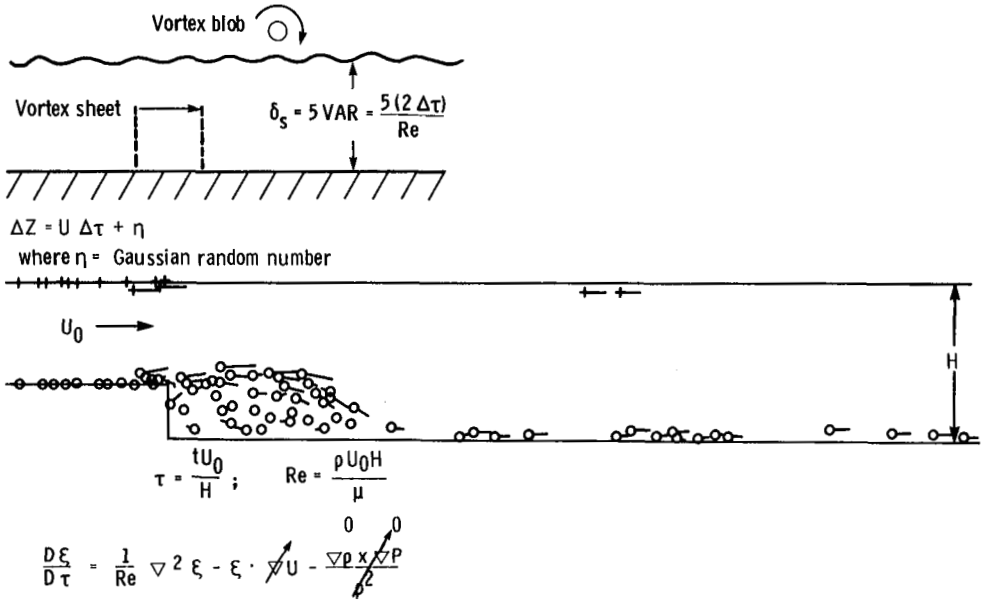

Figure 10. - Modeling interface motion of combustion by Chorin's random vortex method.

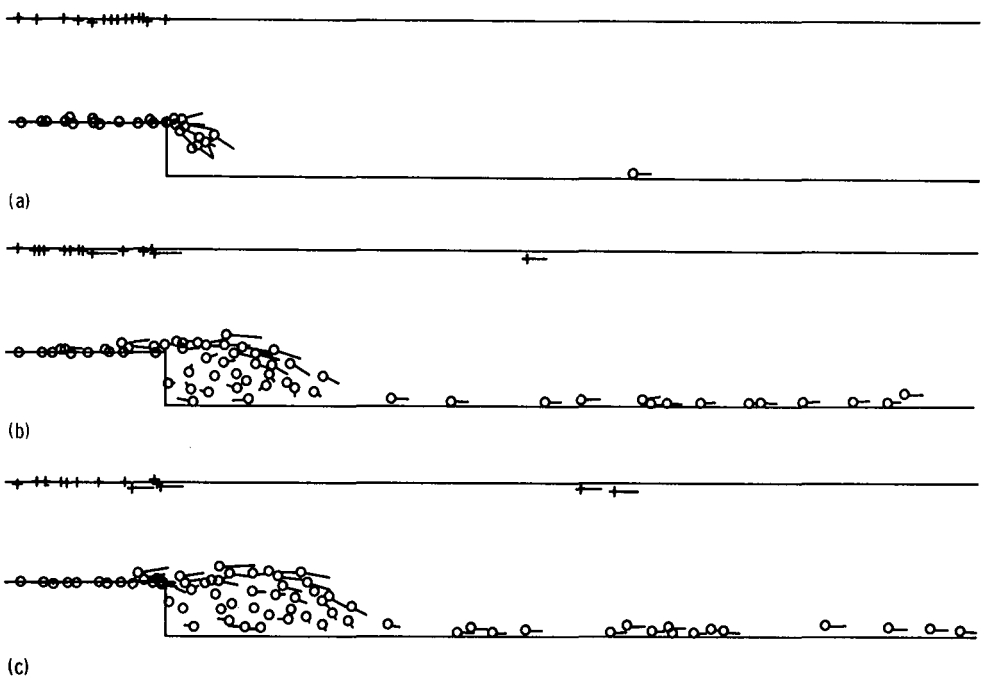

Figure 11. - Motion of vortex blobs computed by Chorin's method. Reynolds number, 10 000.

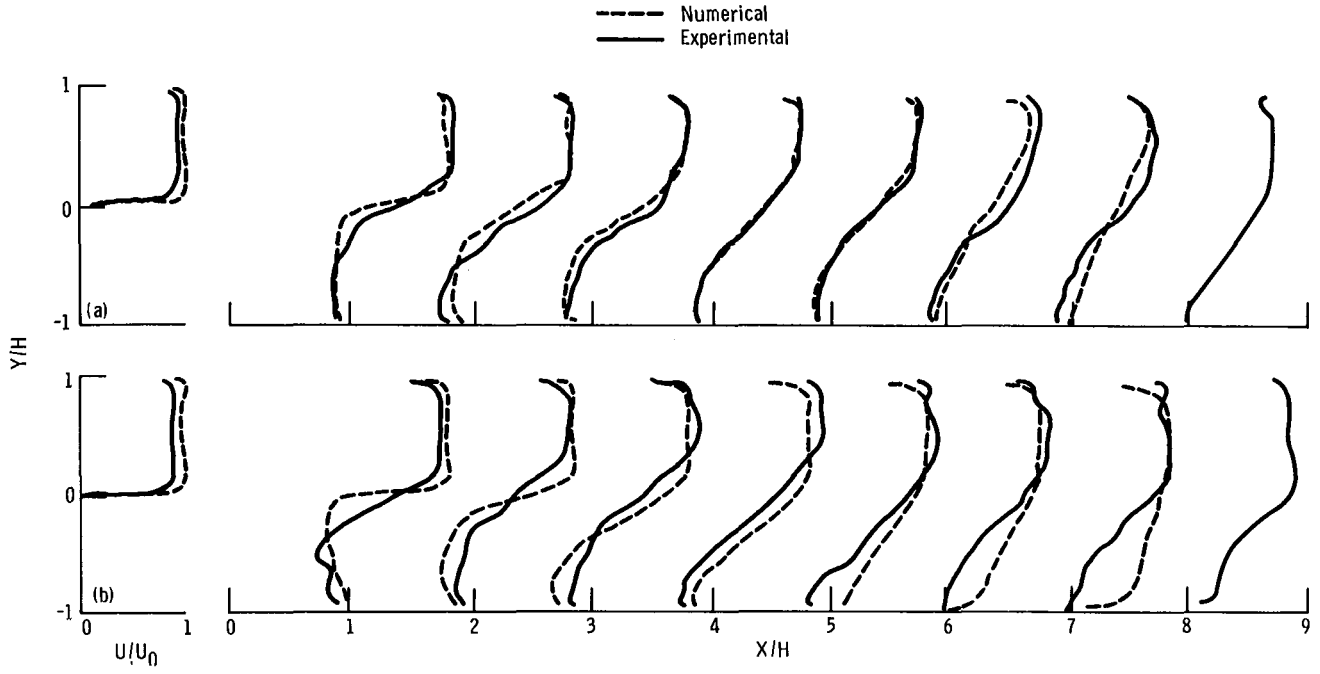

Figure 12. - Comparison of experimental and numerical data for mean velocity.

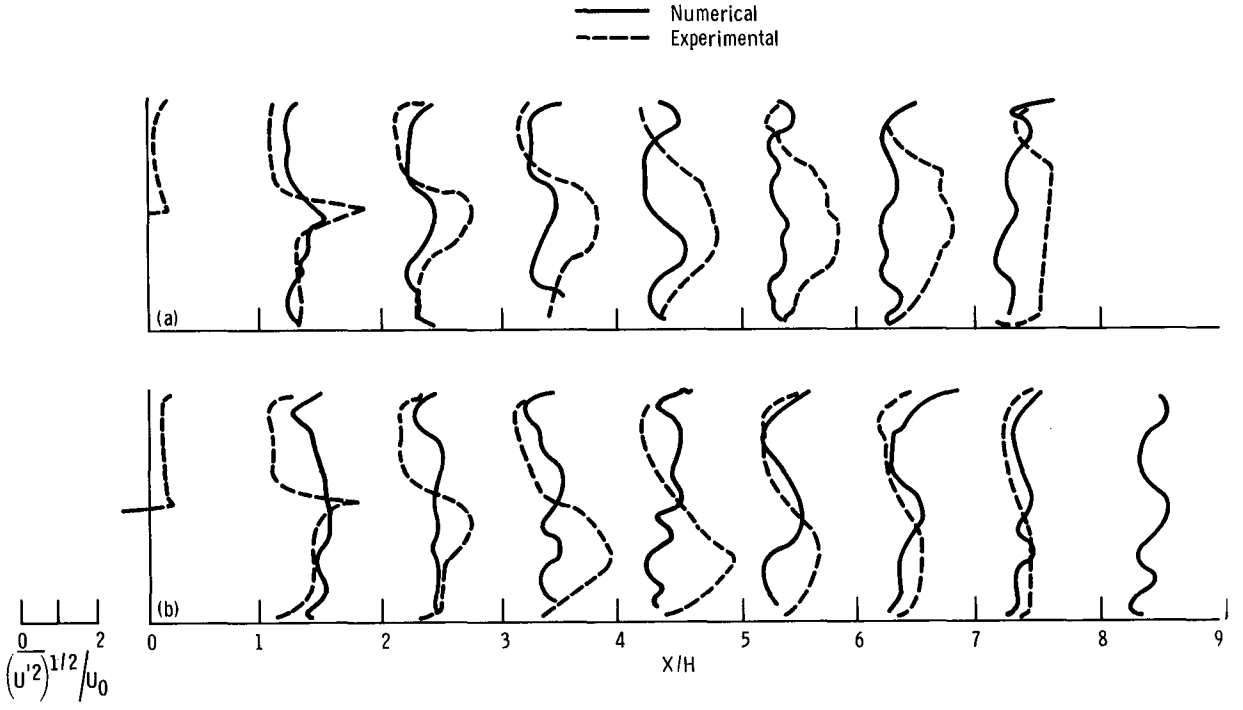

Figure 13. - Comparison of experimental and numerical data for turbulence intensity. (Same configuration as fig. 12.)

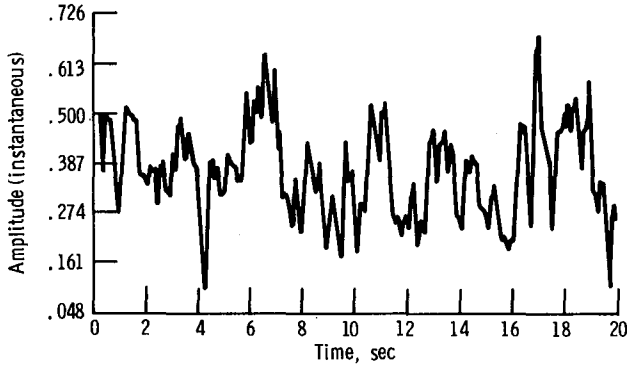

Figure 14. - Instantaneous time history of calculated velocity. x/H = 1.8; Reynolds number, 10 000.

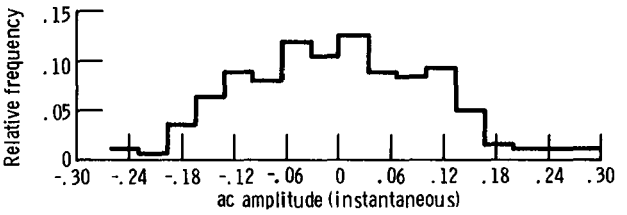

Figure 15. - Computed probability distribution. x/H = 1.8.

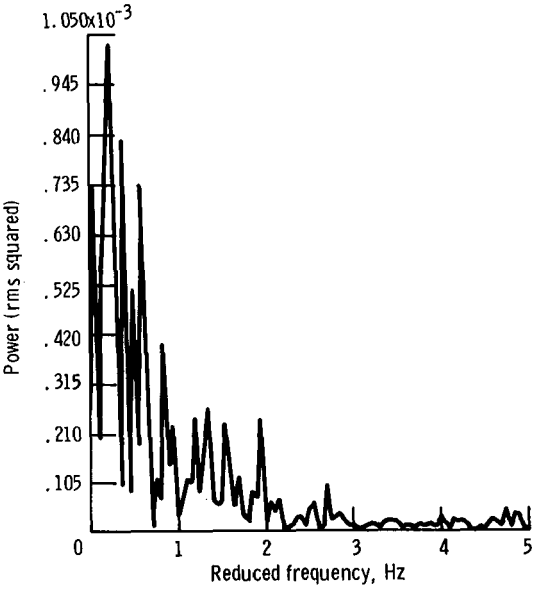

Figure 16. - Computed power spectrum. x/H = 1.8.

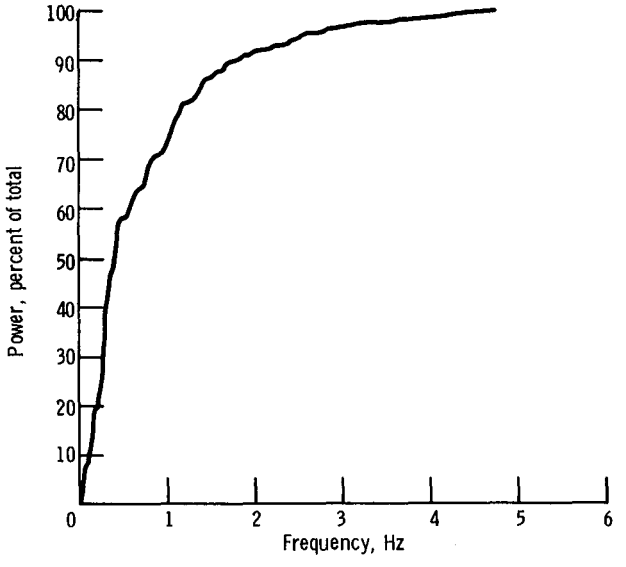

Figure 17. - Power spectral distribution. x/H = 3.6.